Electromagnetic Time Reversal Applied to Fault Location: On the Properties of Back-Injected Signals

Zhaoyang Wang*, Reza Razzaghi†, Mario Paolone‡, and Farhad Rachidi*
* Electromagnetic Compatibility (EMC) Laboratory, {zhaoyang.wang, farhad.rachidi}@epfl.ch
‡ Distributed Energy System Laboratory (DESL), mario.paolone@epfl.ch
Swiss Federal Institute of Technology, EPFL, Lausanne, Switzerland
† Department of Electrical and Computer Systems Engineering, reza.razzaghi@monash.edu
Monash University, Melbourne, Australia

***Abstract*—By using the electromagnetic time reversal (EMTR) theory, the paper studies its properties in order to derive a new fault location method to be used in power networks. It is shown that, in the reversed-time stage, the current signal observed at the true fault location can be clearly distinguished since it appears as a time-delayed copy of the back-injected fault-originated transient signal. Then, based on this similarity property, a fault location method is derived. Finally, the method is numerically validated with reference to a reproducible simulated power network composed of an inhomogeneous multi-conductor transmission-line system.**

***Index Terms*—Cross-correlation sequence, electromagnetic time reversal, electromagnetic transients, fault location, power system.**

I. Introduction

The fault detection and location issue in power system have been extensively studied in literatures for a quite long period of time. Numerous methods and procedures have been developed for both transmission and distribution networks. In general, the existing fault location methodologies are grouped into two main categories: (1) assessing the post-fault impedance (i.e., phasor-based) and (2) analysing the fault-originated high-frequency signals (i.e., travelling-wave based) [1].

In general, the travelling-wave based fault location methods are capable of providing a higher location accuracy compared to the phasor-based ones [2]. Moreover, their performance is less sensitive to the pre-fault conditions as well as the (unknown) fault impedance [3]–[7]. Nevertheless, their practical application is often subject to the use of multiple observation points that may require a suitable time-synchronisation. In addition, when applied to complex topology, these methods may result in non-unique fault locations and, thus, further data processing is required [8].

Recently, to overcome the above-mentioned challenges, a method based on the Electromagnetic Time Reversal (EMTR) theory has been proposed and validated through both reduced- and full-scale experiments (e.g., [9], [10]) as well as various simulation examples making reference to different types of power networks [9], [11]–[13]. Superior performance is provided by this method in terms of high location accuracy and robustness against fault impedance and measurement noise. Later on, using the property of EMTR in changing media, an extension of the EMTR-based fault location method is proposed and validated in [14] and [15]. Compared to the classical method that relies on the matched-media condition to characterise the true fault location with maximum energy concentration, the unmatched media-based procedure focuses on the analysis of the voltage signal observed along the backward-propagation model. In this way, the fault is identified by only a single simulation run, significantly reducing the computation burden that the method developed in [9], [11]–[13] was presenting.

It is worth mentioning that both EMTR-based fault location methods take advantage of the time-reversal invariance of the telegraphers equations in transmission lines. The particular feature of the time-reversal (TR) theory for closed reflecting media enables their application using a single-end measurement [11], which provides the advantage of higher reliability along with lower implementation complexity.

The existing EMTR-based fault location methodologies, considering either matched media or unmatched media, generally devote considerable attention to assessing the features of the signal (e.g., the energy of the fault current signal) observed in the backward-propagation stage (i.e., the reversed-time stage). In contrast, to the best of the Authors knowledge, there is a lack of studies investigating the correlation between the fault-originated transient signal recorded in the direct time and the obtained fault current or voltage in the reversed time.

In this paper, we explore the possibility of using other properties of the EMTR theory to identify the fault location along transmission-line networks. More specifically, we analyse the time-domain similarity between the back-injected transient signal (from the original observation point) and the transverse branch current at guessed fault locations, and propose a similarity-representing index to identify the real fault location.

This work has been supported by the Swiss Competence Center for Energy Research FURIES (Future Swiss Electrical Infrastructure).

The structure of this paper is as follows: Section II discusses the property of time-reversal invariance and its fault location application in power networks. Section III first investigates the EMTR-based similarity characteristic and then formulates a cross-correlation based index to distinguish the real fault location along transmission-line networks. In Section IV, the performance of the proposed method is validated through numerical simulations. Finally, the main contributions made by this paper are summarized in Section V.

II. Time Reversal and its Fault Location Application in Power Networks

A. Time-reversal Invariance

In general, a system is time-reversal (TR) invariant with respect to a physical quantity if, given a solution $f(t)$ to its underlying time-domain differential equations, the time-reversed function $f(-t)$ is also a solution. Since $f(-t)$ is not an experimentally valid solution, in order to ensure the causality requirements, the time-reversed function $f(-t)$ is shifted in time as $f(-t+T)$, where T is the time window in which $f(t)$ is recorded [16].

As the prominent property of a time-reversal invariant system, the time-reversal cavity refers to that the backwards-propagated time-reversed function $f(-t)$ (e.g., acoustic and optic-wave signal) is capable of refocusing on the initial source location. This property has also been experimentally realized by the configuration of time-reversal mirrors (TRM) [17]–[19].

It has been shown that the basic equations of electricity and magnetism, including the telegraphers equations, are time-reversal invariant (in the soft sense) [20].

B. EMTR-Based Fault Location Procedures

The EMTR theory has contributed to propose different methods to locate faults in power networks. Although the fault-indicating metrics are different, the general procedures implementing the methods can be summarised as follows.

- In the direct-time (i.e., forward-propagation) stage, the fault-originated transients are measured at a single observation point.
- In the reversed-time (i.e., backward-propagation) stage, the recorded fault-originated transients are time-reversed and back-injected from the original observation point (using a simulated network model), and fault signals (i.e., current or voltage) are observed at given guessed fault location pre-defined along the network.
- The true fault location can be identified by different metrics, including fault current signal energy (FCSE) [9], fault voltage signal energy (FVSE) [15] and voltage argument (VA) [14].

In the next section, we focus on the analysis of the similarity between the time-domain waveforms of the back-injected transient signal and fault current signal observed at guessed fault locations.

III. EMTR-Based Similarity Characteristic

In this section, we first analyse the similarity between the fault-originated transients recorded and time-reversal operated in the direct-time stage, and the transverse branch currents observed in the reversed-time stage. The analysis is carried out by using the theory of travelling-wave propagation along transmission lines jointly with the EMTR theory. We further argue that the fault current observed at the real fault location can be clearly distinguished since it presents a time-delayed copy of the time-reversed and back-injected transients. Using this argument, a novel EMTR-based fault location method assessing the cross-correlation is proposed.

In order to illustrate the principle of the proposed methodology, we make reference to a simple power network topology composed of a single-conductor transmission line above a ground plane terminated on two power transformers at both ends.

A. Direct-Time Stage: Fault Occurrence

As illustrated in Fig. 1, a post-fault scenario can be modelled by a single-conductor overhead transmission line of length L and an injection of a voltage signal V_f [2]. A single-end measurement is used to carry out the direct-time observation. Specifically, the observation point is placed at $x=0$. Given a fault occurrence at the coordinate $x=x_f$, the fault-originated transients measured at this observation point in the direct time is defined as

$$V_0^{\mathrm{DT}}(t)|_{x_f,\tau} \triangleq V(t,x=0)|_{x_f,\tau}. \tag{1}$$

where τ refers to the time delay associated with travelling-wave propagating from $x=x_f$ to $x=0$ and *vice versa*. Unless otherwise emphasised, $V_0^{\mathrm{DT}}(t)|_{x_f,\tau}$ will be concisely expressed as $V_0^{\mathrm{DT}}(t)$ in what follows.

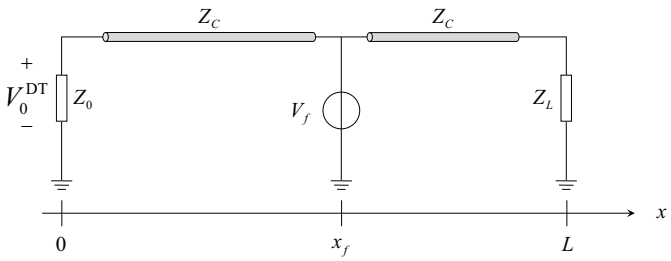

Figure 1: Simplified representation of the post-fault network configuration (in the direct-time stage).

For the sake of simplicity, the line is assumed to be lossless and, therefore, the characteristic impedance Z_C is frequency independent. Note that, it has been shown that the hypothesis of considering a lossless medium does not impact the generality of the EMTR-based fault location method [21]

In addition, the line is considered to be terminated at both ends on power transformers. As discussed in [9], [10] and [14], for the electromagnetic transients characterised by a spectrum with frequencies up to hundreds of kHz, the terminal

$$V_0^{\mathrm{DT}}(t)|_{x_f,\tau} = \begin{cases} 0 & 0 \le t < \tau \\ \left\{(1+\rho_0)\cdot\sum_{i=0}^{N-1}[\rho_0\cdot(-1)]^i\right\}\cdot V_f & (2N-1)\cdot\tau \le t < (2N+1)\cdot\tau \end{cases}, N = 1,2,3,\cdots. \quad (2)$$

transformers can be represented by a high input impedance (resistance), henceforth denoted as Z_0 and Z_L.

A solid fault event in power system is generally described by $V_f(t)$ being a step-like wave [9]. Therefore, the voltage observed at $x = 0$ can be analytically expressed by a piecewise function, given by (2) (see at the top of this page).

In (2), ρ_0 is the voltage reflection coefficient at the observation point $x = 0$, which is defined as

$$\rho_0 = (Z_0 - Z_C)/(Z_0 + Z_C). \quad (3)$$

Similarly, the voltage reflection coefficient at the fault coordinate ρ_{x_f} can be calculated as -1 due to the solid occurrence with zero impedance.

Based on (2), the travelling-wave processes that determine the wave shape of $V_0^{\mathrm{DT}}(t)$ present a damped oscillation time-domain waveform. The amplitude of the voltage wave arriving at $x = 0$ is scaled according to the reflection and transmission effects imposed by the discontinuity at $x = 0$ and $x = x_f$. As previously indicated, in power networks, $\rho_0 \approx +1$. In this paper, for the sake of observability, the damping of the transient processes is accelerated by assuming ρ_0 to be $+0.8$.

From the above consideration, the time-domain waveform of $V_0^{\mathrm{DT}}(t)$ is shown in Fig. 2, where the amplitude of the step-like voltage source V_f is specified as 1 V. It is worth noting that V_f injects the signal at $t = 0$.

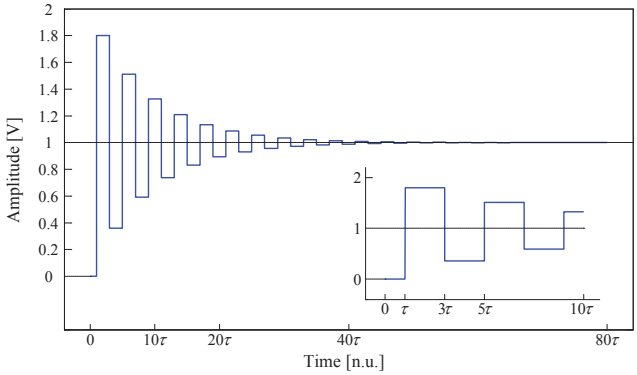

Figure 2: Time-domain waveform of $V_0^{\mathrm{DT}}(t)$ representing the fault-originated transients measured at $x = 0$.

As can be seen in the expanded view in the inset of Fig. 2, the leading edge of the travelling-wave arrives at $x = 0$ after the propagative delay τ. The observed waveform oscillates with a period of 4 τ. In order to ensure that the transients sufficiently damp and $V_0^{\mathrm{DT}}(-t)$ reaches its steady-state value (i.e., 1 V) the waveform is recorded in a duration T of 80 τ.

According to the time-reversal operation described in the previous section, $V_0^{\mathrm{DT}}(-t)$ is reversed and shifted in time, resulting in $V_0^{\mathrm{DT}}(-t+T)$, which will be applied to further procedures to locate the real fault.

B. Reversed-Time Stage: Fault Location

In the reversed-time stage, with the aim of determining the true fault point by observing the fault current flowing through the transverse branch at guessed fault locations, the time-reversed voltage signal $V_0^{\mathrm{DT}}(-t+T)$ is equivalently transformed into the current signal as

$$I_0^{\mathrm{DT}}(t)|_{x_f,\tau} \triangleq I(t, x = 0)|_{x_f,\tau} = V_0^{\mathrm{DT}}(-t+T)/Z_0. \quad (4)$$

and back-injected from the original observation point $x = 0$. Similarly, it will be more frequently represented by $I_0^{\mathrm{DT}}(t)$ henceforth.

The network topology in the reversed-time stage is shown in Fig. 3. For carrying out the back-prorogation simulation, the network topology is modelled in the EMTP-RV environment [22], [23].

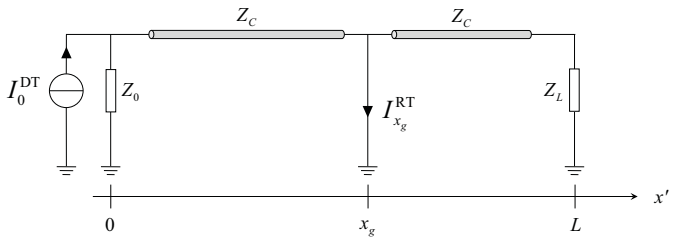

Figure 3: Reversed-time stage network configuration.

The transverse branch current flowing through the guessed fault location $x = x_g$ is defined as

$$I_{x_g}^{\mathrm{RT}}(t) \triangleq I(t, x = x_g). \quad (5)$$

Later in the section, we propose to assess the similarity between the back-injected current $I_0^{\mathrm{DT}}(t)$ and the fault current $I_{x_g}^{\mathrm{RT}}(t)$ by calculating a cross-correlation related index. As known, the cross-correlation assessment relies on the time-domain features that the compared signals demonstrate in a given period (for continuous signals) or with a given number of sampling points (for discrete signals) [24]. For this reason, we observe the waveform of $I_{x_g}^{\mathrm{RT}}(t)$ within a duration of 80 τ, which is exactly same with that of $I_0^{\mathrm{DT}}(t)$.

As assumed before, τ refers to the time delay corresponding to the wave propagation distance between the back-injected point ($x = 0$) and the real fault location $x = x_g = x_f$. Fig. 4 shows the waveforms of $I_{x_g}^{\mathrm{RT}}(t)$ observed at the real fault coordinate and other two non-real fault locations with the

propagative delay respectively being 0.9 τ ($0 < x_g < x_f$) and 1.1 τ ($x_f < x_g < L$), which are close to the true location $x_g = x_f$.

Examining the expanded view of the waveforms in the inset of Fig. 4, it can be seen that the three travelling waves are all characterised as time-reversed damped oscillation processes. Note that the oscillation period is 4 τ, being exactly equal to that of the originally back-injected current $I_0^{\mathrm{DT}}(t)$. More importantly, when x_g coincides with x_f, the fault current signal $I_{x_f}^{\mathrm{RT}}(t)$ retains the waveform features of $I_0^{\mathrm{DT}}(t)$.

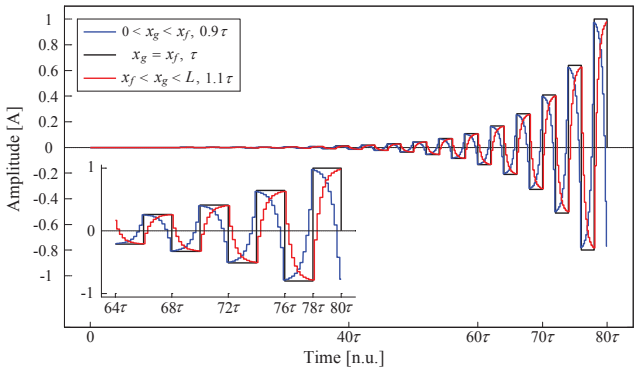

Figure 4: Normalized time-domain waveforms of $I_{x_g}^{\mathrm{RT}}(t)$ respectively measured at $0 < x_g < x_f$, $x_g = x_f$ and $x_f < x_g < L$. The normalization is implemented with reference to the maximum amplitude of $I_{x_g}^{\mathrm{RT}}(t)$.

To further assess the similarity between $I_0^{\mathrm{DT}}(t)$ and $I_{x_f}^{\mathrm{RT}}(t)$, the two current signals are normalized with reference to their respective maximum amplitude and shown in Fig. 5. It can be clearly seen that $I_{x_f}^{\mathrm{RT}}(t)$ is a copy of $I_0^{\mathrm{DT}}(t)$ being positively shifted in time by the delay τ.

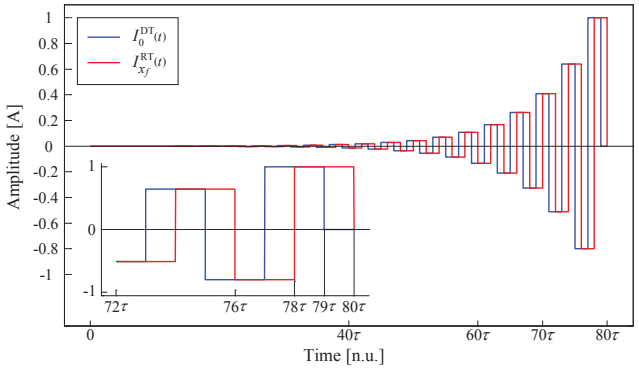

Figure 5: Normalized time-domain waveforms of $I_0^{\mathrm{DT}}(t)$ and $I_{x_f}^{\mathrm{RT}}(t)$.

In this example, we presented the observation at non-real fault locations only for two specific points (i.e., with a time delay of 0.9 τ and 1.1 τ). However, it is worth mentioning that, in view of travelling-wave propagation, the real fault location is characterised as a unique point along the line satisfying that the wave propagative distances in both stages (i.e., the direct-time and reversed-time) are absolutely identical.

Based on the above-mentioned fault scenario, we have observed that the most significant time-domain similarity (or the highest cross-correlation) between $I_0^{\mathrm{DT}}(t)$ and $I_{x_g}^{\mathrm{RT}}(t)$ is obtained when $x_g \equiv x_f$. In what follows, we will further verify the observation by introducing a cross-correlation sequence based index, quantifying the degrees of the similarity.

C. Similarity index

In this subsection, we formulate a similarity index based on the calculation of cross-correlation sequence of discrete sampled signals. To this end, we first discretise $I_0^{\mathrm{DT}}(t)$ and $I_{x_g}^{\mathrm{RT}}(t)$ respectively as

$$\phi(k) \triangleq I_0^{\mathrm{DT}}(k \cdot \Delta t)|_{x_f,\tau}, \quad k = 0,1,2,\cdots,K. \tag{6}$$

and

$$\psi(x_g,k) \triangleq I_{x_g}^{\mathrm{RT}}(k \cdot \Delta t)|_{x_f,\tau}, \quad k = 0,1,2,...,K. \tag{7}$$

where, Δt refers to the time-sampled interval, and K is the number of samples, which is determined by the flooring operation that

$$K = floor(T/\Delta t). \tag{8}$$

Given this, the maximum of the cross-correlation sequence of $\phi(k)$ and $\psi(x_g,k)$c is calculated by

$$R_{\phi,\psi}^{m}(x_g,l) = max\left\{\sum_{k=0}^{K}\left\langle \underset{max[\phi(k)]}{nor}[\phi(k)]\right\rangle \cdot \left\langle \underset{max[\phi(k)]}{nor}[\psi(x_g,k-l)]\right\rangle\right\}, \tag{9}$$

$$l = 0,\ \pm 1,\ \pm 2,\ \cdots,\ \pm(K-1).$$

where, the operation $nor[]$ means normalising the sequences with respect to the maximum of $\phi(k)$ (i.e., the maximum of the time-discrete sampled and back-injected transients $I_0^{\mathrm{DT}}(t)$).

Among all the guessed fault locations, the real fault coordinate x_f can be inferred from

$$x_f = arg|_{x_g}\ max\left\{R_{\phi,\psi}^{m}(x_g,l)\right\}. \tag{10}$$

Recalling the scenario considered in the previous subsections, we apply the proposed method to quantifying the similarity between $I_0^{\mathrm{DT}}(t)$ and $I_{x_g}^{\mathrm{RT}}(t)$. In this example, the distances between the observation point and the guessed fault locations are represented by the normalised pattern being their respective propagative delay. In particular, the line length L corresponds to a delay of 2.4 τ. As can be seen from the results shown in Fig. 6, that the highest cross-correlation occurs at the real fault location is readily proved by the maximum value of the formulated index.

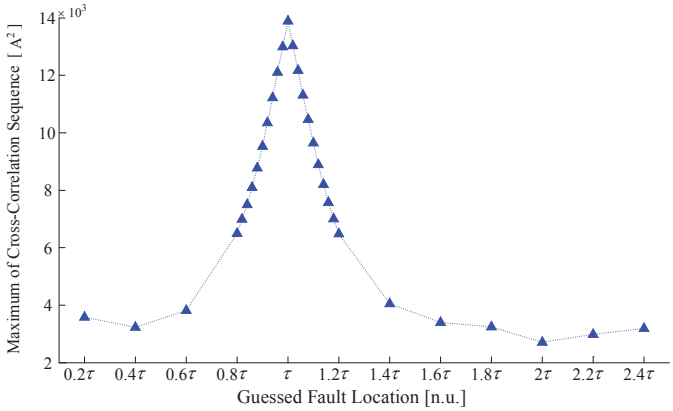

Figure 6: Maximum of the cross-correlation sequence calculated at the guessed fault locations along the line of Fig. 3.

So far, the proposed time-domain similarity characteristic has been introduced and verified by considering a single-conductor overhead transmission line. Moreover, a cross-correlation sequence-based fault location method has been proposed. In the next section, we will present the performance validation of the proposed method by making reference to a more complex power grid topology in the simulation environment of EMTP-RV.

IV. Numerical Validation of the EMTR-based Fault Location Method Using the Similarity Index

In this section, we numerically validate the proposed similarity Index and the cross-correlation sequence-based fault location method by making reference to an inhomogeneous multi-conductor configuration.

To be specific, the tested system is a 230 kV three-phase network composed of an overhead line and an underground cable. As shown in Fig. 7, the overhead line is 9 km long and the underground cable is 3 km long. Using typical geometrical and electrical parameters of 230 kV lines and cables, the network is modelled in the EMTP-RV simulation environment by using a constant-parameter (CP) line module. The use of the CP line module to investigate the general fault-associated electromagnetic-transient process in power systems has been justified in [9].

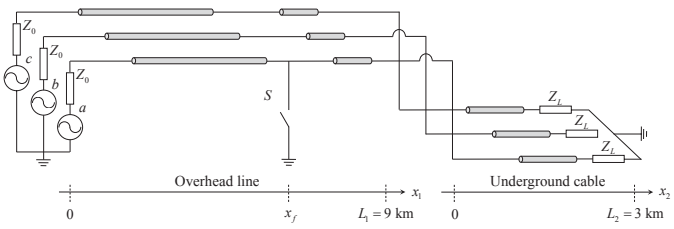

Figure 7: Schematic representation of the 230 kV three-phase power network adopted as a test case.

The series impedance and shunt admittance matrices for the adopted line and cable are calculated, corresponding to their respective switching frequency (see [9] to infer the relevant line/cable parameters and reproduce the paper findings). It should also be noted that the inductive and capacitive coupling effects between phases are taken into consideration by the CP line module.

Based on the assumption presented earlier, the network is considered to be terminated on power transformers, thus in the simulation, each end of the phase conductor is connected to a lumped impedance element. The value of the impedance is large enough compared to the characteristic impedance of the line/cable (in the order of hundreds of ohm). In particular, Z_0 and Z_L are set to 100 kΩ. In addition, the three-phase fault-originated transients are synchronously evaluated at the line end (i.e., $x_1 = 0$), where a 230 kV three-phase AC voltage source supplies the network. As for the fault case, we assume that a single phase (i.e., phase a) to ground fault occurs at $x_1 = x_f = 7$ km, namely at 7 km away from the observation point.

Using the same nomenclature given in the previous section, we express the sequence of fault-originated transients with respect to observed phase (abbreviated as ph referring to phase a, b and c of Fig. 7) as

$$V_{0,ph}^{\mathrm{DT}}(-k\cdot\Delta t + K). \tag{11}$$

In the reversed-time stage, with reference to the corresponding phase, the sequence of back-injected three-phase current is similarly obtained as

$$I_{0,ph}^{\mathrm{DT}}(k\cdot\Delta t). \tag{12}$$

To identify the true fault location, the fault current is measured at each guessed fault location (i.e., every 1 km along each phase). Moreover, in order to evaluate the performance of the proposed method in terms of location accuracy, the distance step is reduced to 200 m between $x_1 = 6$ km and $x_1 = 8$ km, the 1 km span before and after the fault coordinate. We denote the sequence of the fault current observed at guessed fault location x_g along each phase as

$$I_{x_g,ph}^{\mathrm{RT}}(k\cdot\Delta t). \tag{13}$$

Fig. 8 presents the back-injected current signal to the faulty phase a and the current observed at the real fault location (also here, the normalisation has been implemented with respect to their respective maximum amplitude). As it can be observed from the detailed (superimposed) comparison shown in Fig. 8 (c), the proposed similarity characteristics still hold in this inhomogeneous power network. Note that, although the losses are taken into account in this case study, the presence of losses does not significantly impact the similarity between two waveforms.

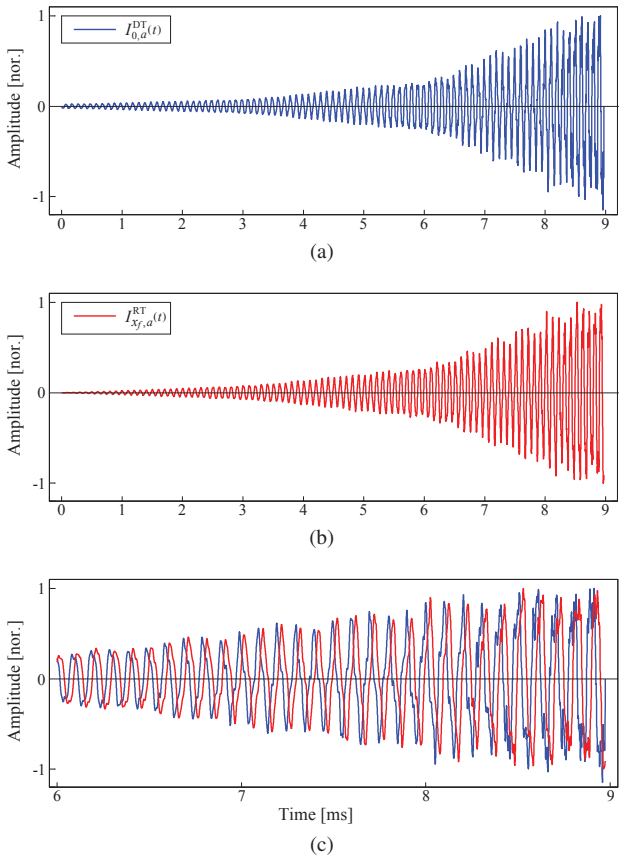

Figure 8: Normalised time-domain waveforms of (a) the current signal back injected to the faulty phase a, and (b) the current observed at the real fault location corresponding to the configuration of Fig. 7. (c) Detailed observation of the similarity between (a) and (b), which are superimposed on the same plot.

Instead of graphically comparing the back-injected transient current and fault current measured at non-real fault locations along the network, we quantify the degrees of the similarity by calculating the cross-correlation sequence of (12) and (13).

According to the similarity index proposed in (9), the maximum of the cross-correlation sequence of (12) and (13) is described as a function of the guessed fault location and illustrated in Fig. 9. It evidently shows that the highest cross-correlation occurs at the real fault location even in an inhomogeneous multi-conductor configuration.

Furthermore, both the faulty phase and fault location are accurately distinguished by the maximum among the calculated indexes. In other words, the proposed method is able to identify the faulty phase and the real fault coordinate along the conductor of the faulty phase.

From the above, the index presented in (9) is verified through the case study simulating a realistic inhomogeneous multi-conductor power network.

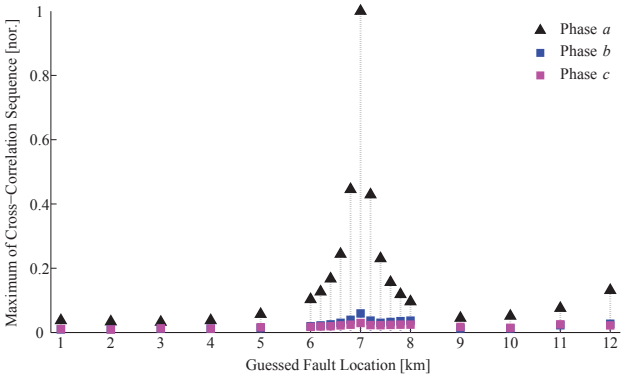

Figure 9: Normalised similarity index based on calculating the maximum of the cross-correlation sequence of back-injected transients and fault current measured at guessed fault locations. The normalization is implemented with reference to the maximum of the index.

V. Conclusions

In this paper, with the aim of deriving a new EMTR-based fault location method in power system, we analysed the similarity between the back-injected fault-originated transient signal and the fault current signal at guessed fault locations. It has been shown that the current flowing through the transverse branch at the true fault location is characterised as a time-delayed copy of the originally-injected transients.

By defining a cross-correlation sequence based-index quantitatively representing the similarity, a new EMTR-based fault location method was derived. With reference to an inhomogeneous multi-conductor transmission-line network, the proposed similarity-based fault location method has also been numerically validated.

References

[1] *IEEE Guide for Determining Fault Location on AC Transmission and Distribution Lines*. IEEE Std. C37.114-2014 (Revision of IEEE Std C37.114-2004), Jan 2015.

[2] *Protection of Distribution Systems with Distributed Energy Resources*. CIGRE Joint working group B5-C6 (26), 2015.

[3] A. Borghetti, M. Bosetti, M. Di Silvestro, C. A. Nucci, and M. Paolone, "Continuous-wavelet transform for fault location in distribution power networks: Definition of mother wavelets inferred from fault originated transients," *IEEE Transactions on Power Systems*, vol. 23, no. 2, pp. 380–388, 2008.

[4] A. Borghetti, M. Bosetti, C. Nucci, M. Paolone, and A. Abur, "Integrated use of time-frequency wavelet decompositions for fault location in distribution networks: Theory and experimental validation," *IEEE Transactions on Power Delivery*, vol. 25, no. 4, pp. 3139–3146, 2010.

[5] F. H. Magnago and A. Abur, "Fault location using wavelets," *IEEE Transactions on Power Delivery*, vol. 13, no. 4, pp. 1475–1480, 1998.

[6] F. Lopes, D. Fernandes, and W. Neves, "A traveling-wave detection method based on park's transformation for fault locators," *IEEE Transactions on Power Delivery*, vol. 28, no. 3, pp. 1626–1634, 2013.

[7] S. Azizi, M. Sanaye-Pasand, M. Abedini, and A. Hasani, "A traveling-wave-based methodology for wide-area fault location in multiterminal dc systems," *IEEE Transactions on Power Delivery*, vol. 29, no. 6, pp. 2552–2560, 2014.

[8] M. M. Saha, J. J. Izykowski, and E. Rosolowski, *Fault location on power networks*. Springer Science & Business Media, 2009.

[9] R. Razzaghi, G. Lugrin, H. Manesh, C. Romero, M. Paolone, and F. Rachidi, "An efficient method based on the electromagnetic time reversal to locate faults in power networks," *IEEE Transactions on Power Delivery*, vol. 28, no. 3, pp. 1663–1673, 2013.

[10] Z. Wang, S. He, Q. Li, B. Liu, R. Razzaghi, M. Paolone, Y. Xie, M. Rubinstein, and F. Rachidi, "A full-scale experimental validation of electromagnetic time reversal applied to locate disturbances in overhead power distribution lines," *IEEE Transactions on Electromagnetic Compatibility*, vol. PP, no. 99, pp. 1–9, 2018.

[11] R. Razzaghi, F. Rachidi, and M. Paolone, "Single-end FPGA-based fault location system for radial/meshed AC/DC networks based on the electromagnetic time reversal theory," in *PowerTech, 2017 IEEE Manchester*, pp. 1–7, IEEE, 2017.

[12] R. Razzaghi, G. Lugrin, M. Paolone, and F. Rachidi, "On the use of electromagnetic time reversal to locate faults in series-compensated transmission lines," in *PowerTech, 2013 IEEE Grenoble*, pp. 1–5, IEEE, 2013.

[13] R. Razzaghi, M. Paolone, F. Rachidi, J. Descloux, B. Raison, and N. Retière, "Fault location in multi-terminal hvdc networks based on electromagnetic time reversal with limited time reversal window," in *Power Systems Computation Conference (PSCC), 2014*, pp. 1–7, IEEE, 2014.

[14] A. Codino, Z. Wang, R. Razzaghi, M. Paolone, and F. Rachidi, "An alternative method for locating faults in transmission line networks based on time reversal," *IEEE Transactions on Electromagnetic Compatibility*, vol. 59, no. 5, pp. 1601–1612, 2017.

[15] Z. Wang, A. Codino, R. Razzaghi, M. Pacione, and F. Rachidi, "Using electromagnetic time reversal to locate faults in transmission lines: Definition and application of the mirrored minimum energy property," in *EMC EUROPE, 2017 International Symposium on Electromagnetic Compatibility*, pp. 1–6, IEEE, 2017.

[16] F. Rachidi, M. Rubinstein, and M. Paolone, *Electromagnetic Time Reversal: Application to EMC and Power Systems*. John Wiley & Sons, 2017.

[17] M. Fink, "Time reversal of ultrasonic fields. i. basic principles," *IEEE transactions on ultrasonics, ferroelectrics, and frequency control*, vol. 39, no. 5, pp. 555–566, 1992.

[18] F. Wu, J.-L. Thomas, and M. Fink, "Time reversal of ultrasonic fields. il. experimental results," *IEEE transactions on ultrasonics, ferroelectrics, and frequency control*, vol. 39, no. 5, pp. 567–578, 1992.

[19] D. Cassereau and M. Fink, "Time-reversal of ultrasonic fields. iii. theory of the closed time-reversal cavity," *IEEE transactions on ultrasonics, ferroelectrics, and frequency control*, vol. 39, no. 5, pp. 579–592, 1992.

[20] M. Rubinstein, F. Rachidi, and M. Paolone, *Time reversal: A different perspective*, pp. 1–27. John Wiley & Sons, 2017.

[21] R. Razzaghi, G. Lugrin, F. Rachidi, and M. Paolone, "Assessment of the influence of losses on the performance of the electromagnetic time reversal fault location method," *IEEE Transactions on Power Delivery*, vol. 32, no. 5, pp. 2303–2312, 2017.

[22] H. W. Dommel, "Digital computer solution of electromagnetic transients in single-and multiphase networks," *IEEE transactions on power apparatus and systems*, no. 4, pp. 388–399, 1969.

[23] J. Mahseredjian, S. Dennetière, L. Dubé, B. Khodabakhchian, and L. Gérin-Lajoie, "On a new approach for the simulation of transients in power systems," *Electric power systems research*, vol. 77, no. 11, pp. 1514–1520, 2007.

[24] J. G. Proakis and D. G. Manolakis, *Digital signal processing: principles, algorithms, and applications*. Pearson Prentice Hall, 2007.